Electronic Supplementary Material (ESI) for Materials Chemistry Frontiers.
This journal is © the Partner Organisations 2023

Electronic Supplementary Information

Fluorescence quenching mechanism of tetrazine-functionalized fluorogenic labels with integrated π-conjugations: internal conversion to a dark state

Tianruo Shen,[a] *Wenda Zhang*,[a,b] *Priya Yadav*,[a] *Xiao Wei Sun*[b] *and Xiaogang Liu**,[a]

[a] Science, Mathematics, and Technology Cluster, Singapore University of Technology and Design, 8 Somapah Road, Singapore 487372, Singapore.

[b] Institute of Nanoscience and Applications and Department of Electrical and Electronic Engineering, Southern University of Science and Technology, Shenzhen 518055, China.

* Corresponding Author: Xiaogang Liu (xiaogang_liu@sutd.edu.sg)

Contents

Experimental Conditions for the Reported Tetrazine-Based Fluorogenic Labels

The testing conditions for the reported tetrazine-based fluorogenic probes are listed in Table S1. Two dienophiles, *trans*-cyclooctene (**TCO**), and bicyclononyne (**BCN**), were reacted with different probes in various media.

Table S1. Experimental conditions for five sets of molecules.

Set	React with	Medium	Reference
1	**TCO**	Acetonitrile (ACN):water = 1:1	Park *et al.*[1]
2	**TCO**	ACN:water = 1:1	Park *et al.*[1]
3	**BCN**	ACN:HEPES = 1:1	Kele *et al.*[2]
4	**BCN**	Ethanol (EtOH)	Wu *et al.*[3]
5	**BCN**	Acetonitrile	Vrabel *et al.*[4]

Computational Methods

The density functional theory (DFT) and time-dependent DFT (TD-DFT) calculations were carried out in the *Gaussian 16* program.[5-7] All the calculations were performed using ωB97XD functional and def-2SVP basis set.[8, 9] We considered the solvation effects by deploying the SMD solvent model and linear-response (LR) solvent formalism in EtOH.[10-12] All the optimized molecular structures at the ground and excited states were confirmed at the local minimums of the potential energy surfaces of S_0, S_1, and S_2. The Avogadro software was applied to visualize the optimized geometries of all molecules.[13] The hole-electron analyses were performed and visualized using Multiwfn and VMD software.[14-17]

Additional Computational Results

Establishment of the Internal Conversion to a Dark State (ICDS) Model

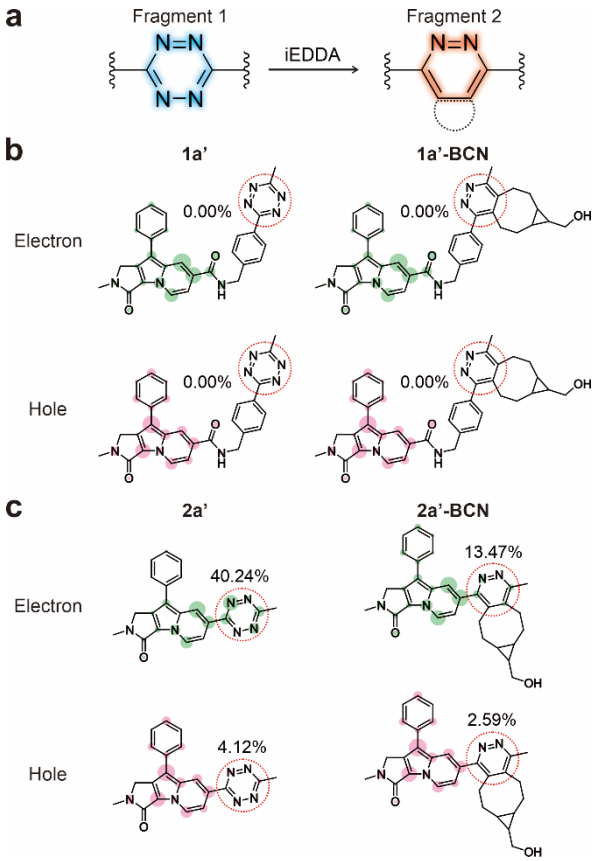

Fig. S1 (a) Two representative fragments extracted from the precursors and products for analyzing the fragment contributions to the electron and hole distributions. (b) Atomic contributions to the hole-electron distributions of the bright states for **1a'**/**1a'-BCN** and (c) **2a'**/**2a'-BCN**. The inset values show the fragment contributions to the hole or electron distributions.

To quantify the fragment contributions to the hole (η_H) and electron (η_E) distributions of different states, we calculated the contributions of Fragment 1 to the labels and Fragment 2 to the products, respectively (Fig. S1). The results indicated that Fragment 1 has participated in the π-π* transitions of the bright state in **2a'**, and Fragment 2 has joined the π-π* transitions of the bright states in **2a'-BCN**.

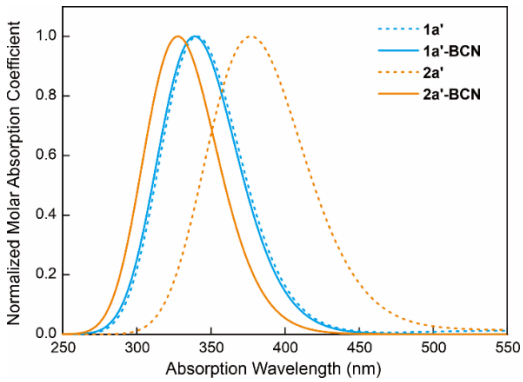

Fig. S2 Calculated UV-vis absorption spectra of **1a'**, **1a'-BCN**, **2a'**, and **2a'-BCN**.

To rationalize the ICDS mechanism of tetrazine-derived fluorophores with integrated π-conjugations, we carried out the ground state geometric optimizations and electronic structure analysis, *i.e.*, vertical excitation energy, hole-electron distribution, and charge transfer distance (d_{CT}), and fragment contribution, for various probes and their products upon reactions with **BCN** (Fig. S3-S14). The same quenching mechanism (ICDS) for these precursors was obtained.

We observed a low-lying dark state with ~0 oscillator strength (*f*) in all precursor dyes. This dark state was eliminated after iEDDA reactions, as reflected by large *f* values in all products.

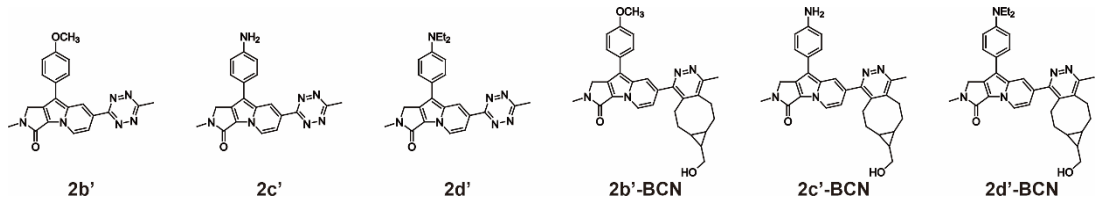

Fig. S3 Molecular structures of **2b'**, **2c'**, **2d'**, **2b'-BCN**, **2c'-BCN**, and **2d'-BCN**.

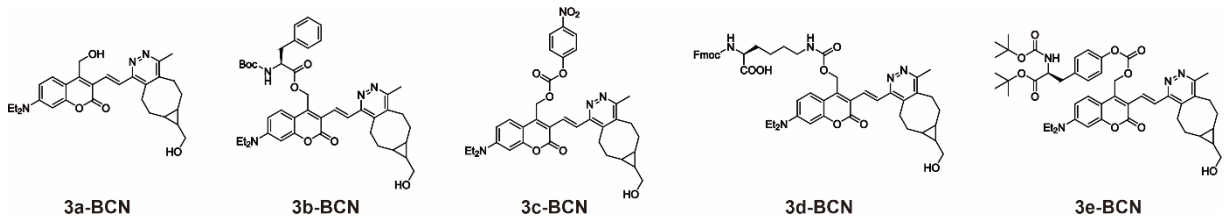

Fig. S4 Molecular structures of Set 3 molecules after reacting with **BCN**.

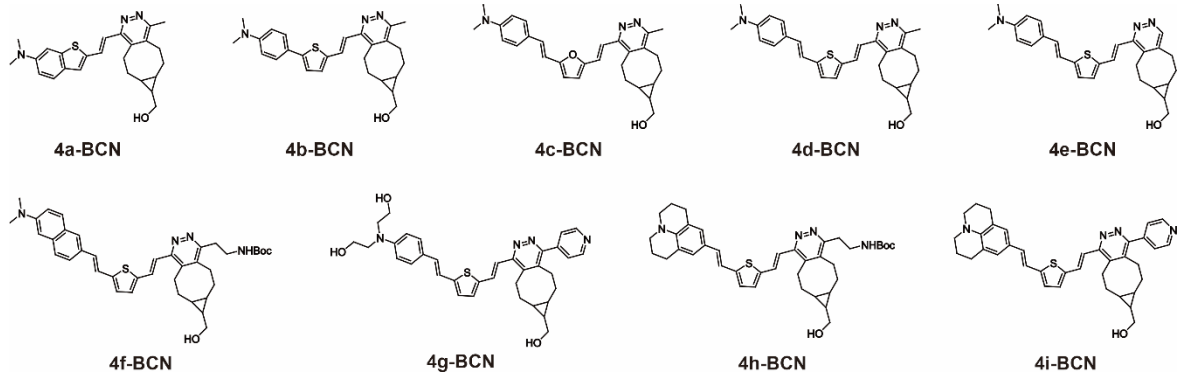

Fig. S5 Molecular structures of Set 4 molecules after reacting with **BCN**.

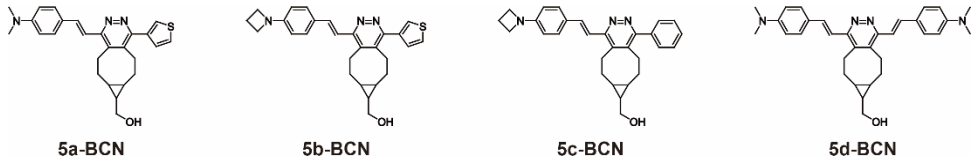

Fig. S6 Molecular structures of Set 5 molecules after reacting with **BCN**.

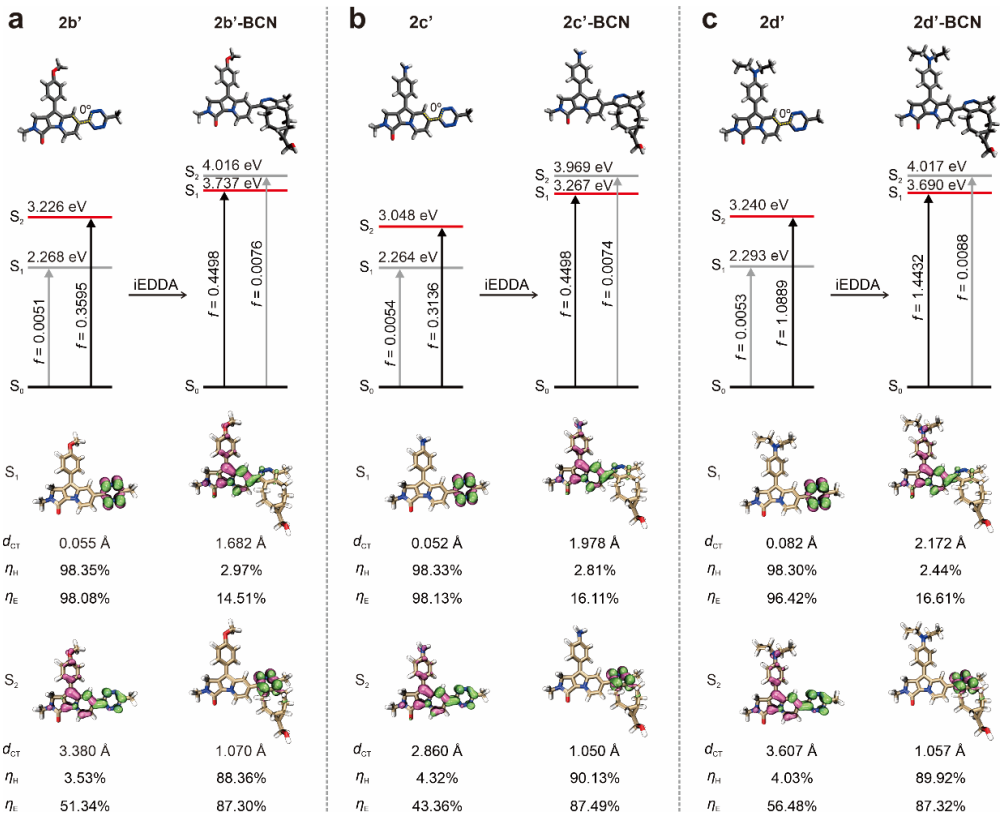

Fig. S7 Optimized geometries (top), energy levels of key states during the vertical excitation processes (middle), and corresponding hole-electron distributions (mauve: hole; green: electron) with d_{CT}, η_H, and η_E (bottom) of (a) **2b'/2b'-BCN**, (b) **2c'/2c'-BCN**, and (c) **2d'/2d'-BCN**.

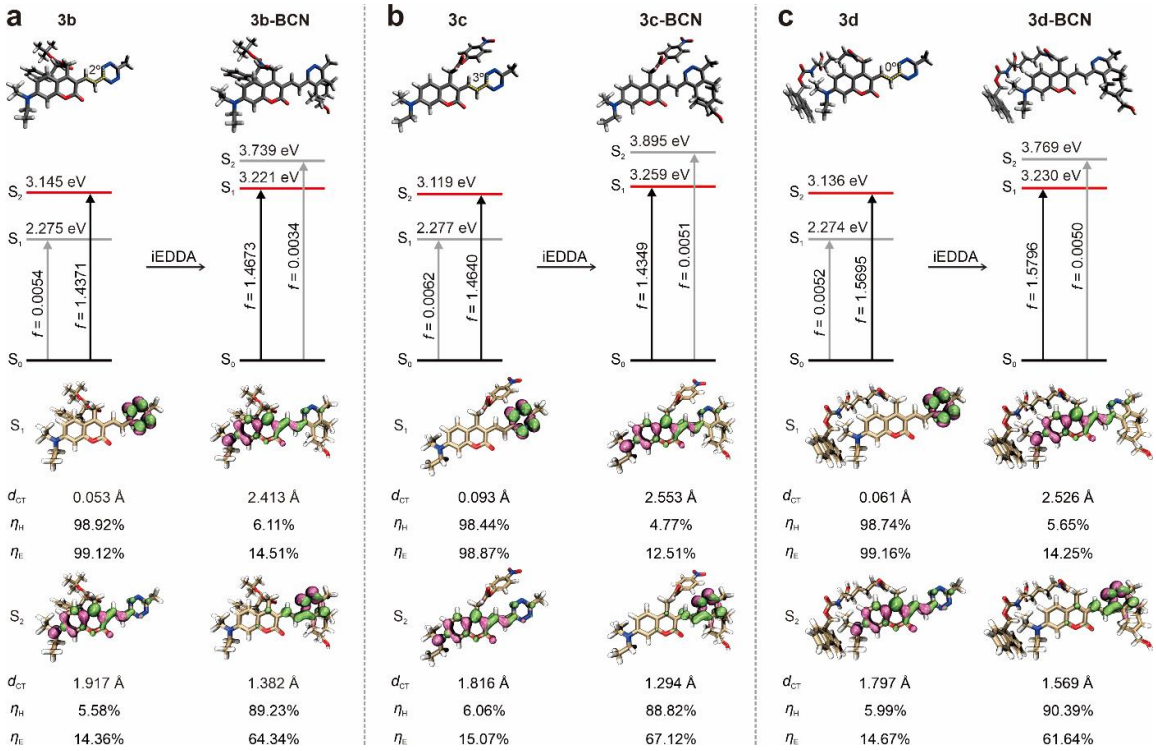

Fig. S8 Optimized geometries (top), energy levels of key states during the vertical excitation processes (middle), and corresponding hole-electron distributions (mauve: hole; green: electron) with d_{CT}, η_H, and η_E (bottom) of (a) **3b/3b-BCN**, (b) **3c/3c-BCN**, and (c) **3d/3d-BCN**.

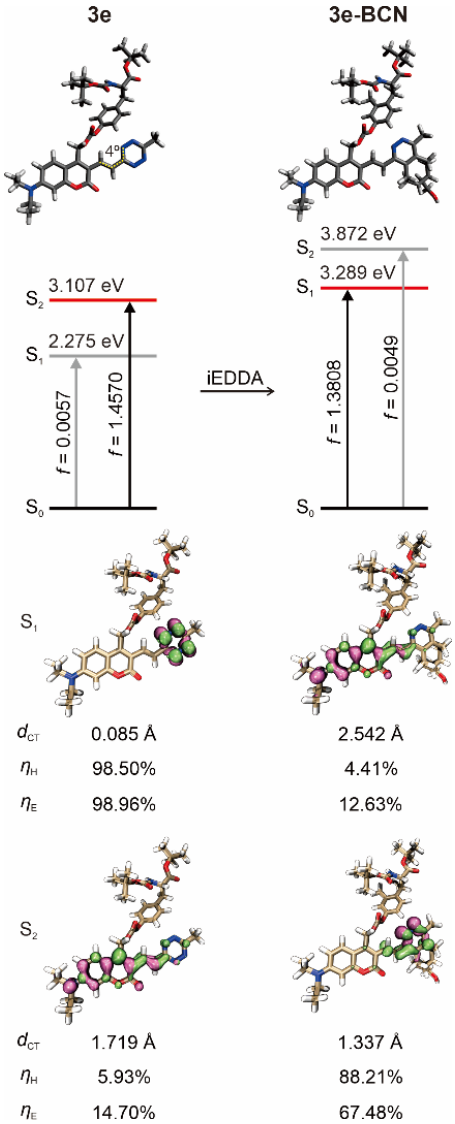

Fig. S9 Optimized geometries (top), energy levels of key states during the vertical excitation processes (middle), and corresponding hole-electron distributions (mauve: hole; green: electron) with d_{CT}, η_H, and η_E (bottom) of **3e/3e-BCN**.

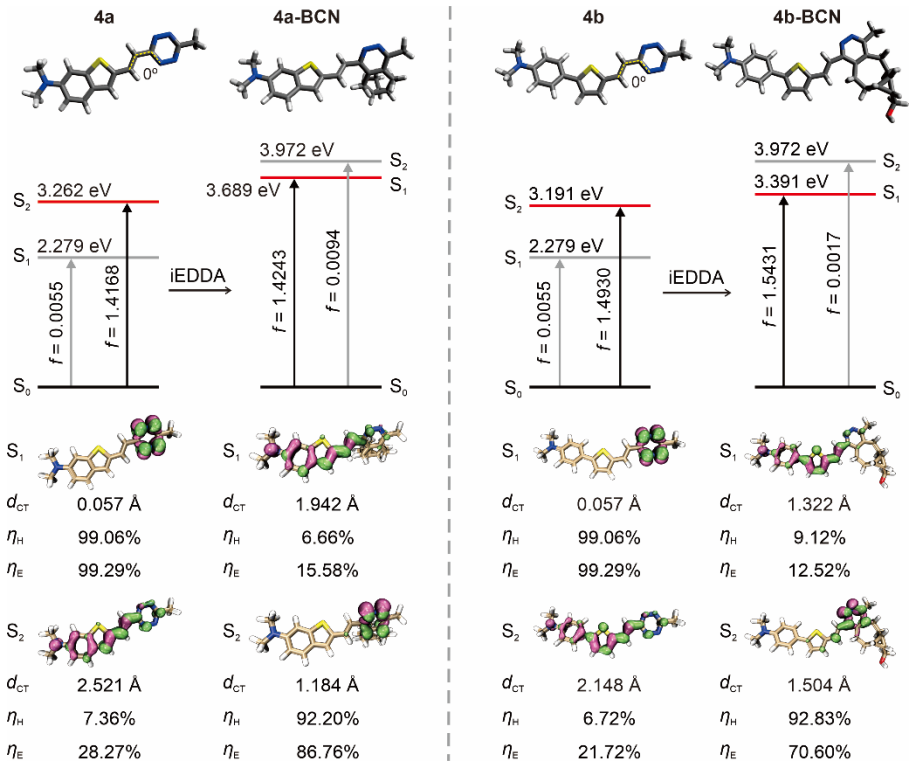

Fig. S10 Optimized geometries (top), energy levels of key states during the vertical excitation processes (middle), and corresponding hole-electron distributions (mauve: hole; green: electron) with d_{CT}, η_H, and η_E (bottom) of **4a**/**4a-BCN** (left) and **4b**/**4b-BCN** (right).

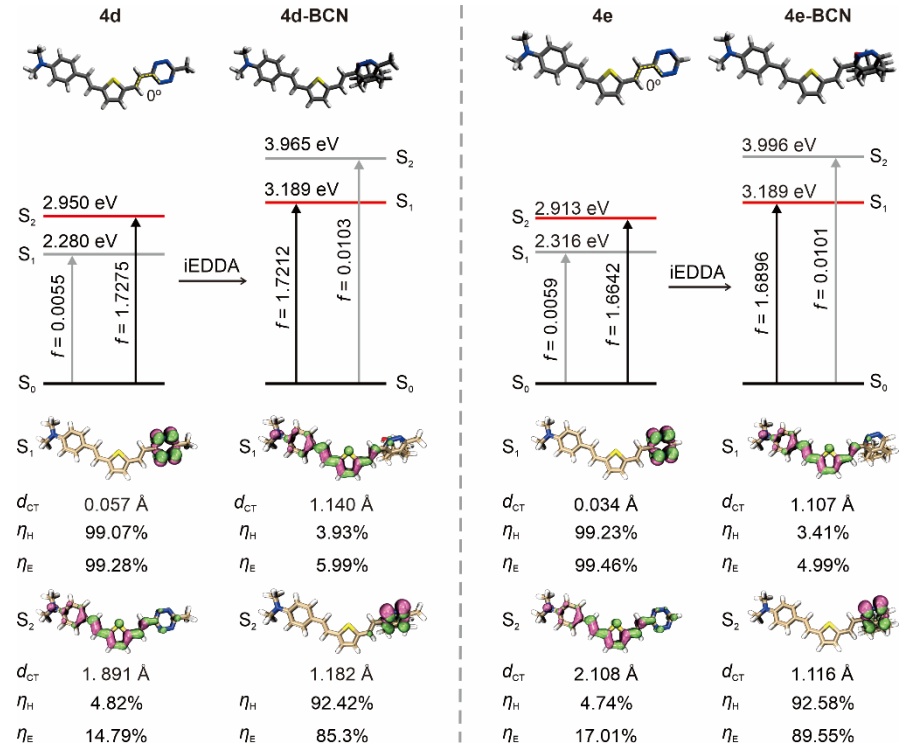

Fig. S11 Optimized geometries (top), energy levels of key states during the vertical excitation processes (middle), and corresponding hole-electron distributions (mauve: hole; green: electron) with d_{CT}, η_H, and η_E (bottom) of **4d**/**4d-BCN** (left) and **4e**/**4e-BCN** (right).

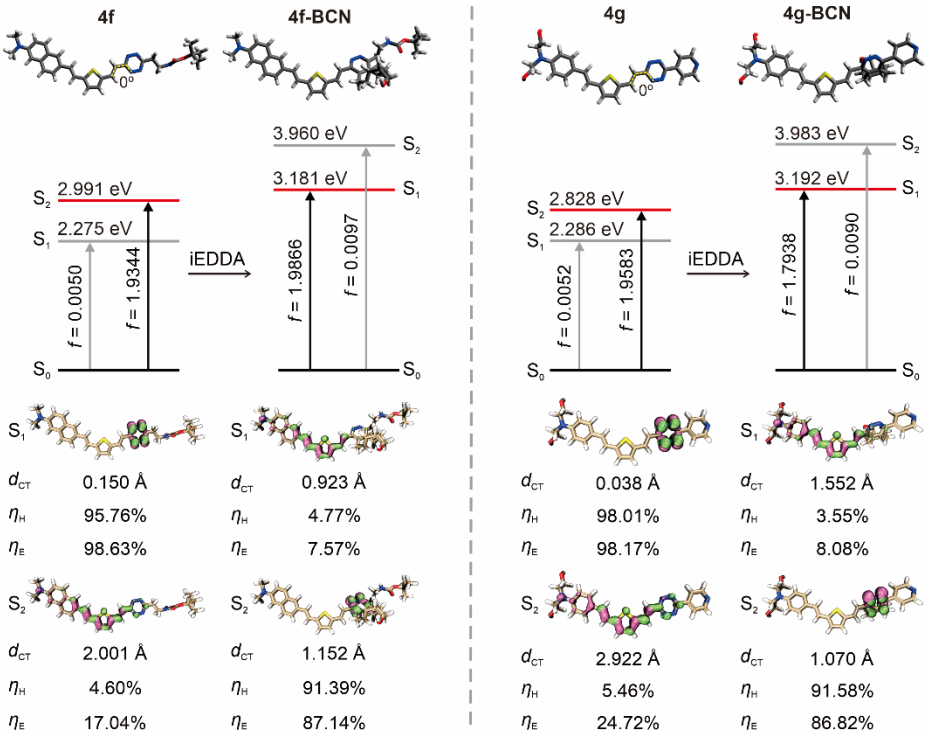

Fig. S12 Optimized geometries (top), energy levels of key states during the vertical excitation processes (middle), and corresponding hole-electron distributions (mauve: hole; green: electron) with d_{CT}, η_H, and η_E (bottom) of **4f**/**4f-BCN** (left) and **4g**/**4g-BCN** (right).

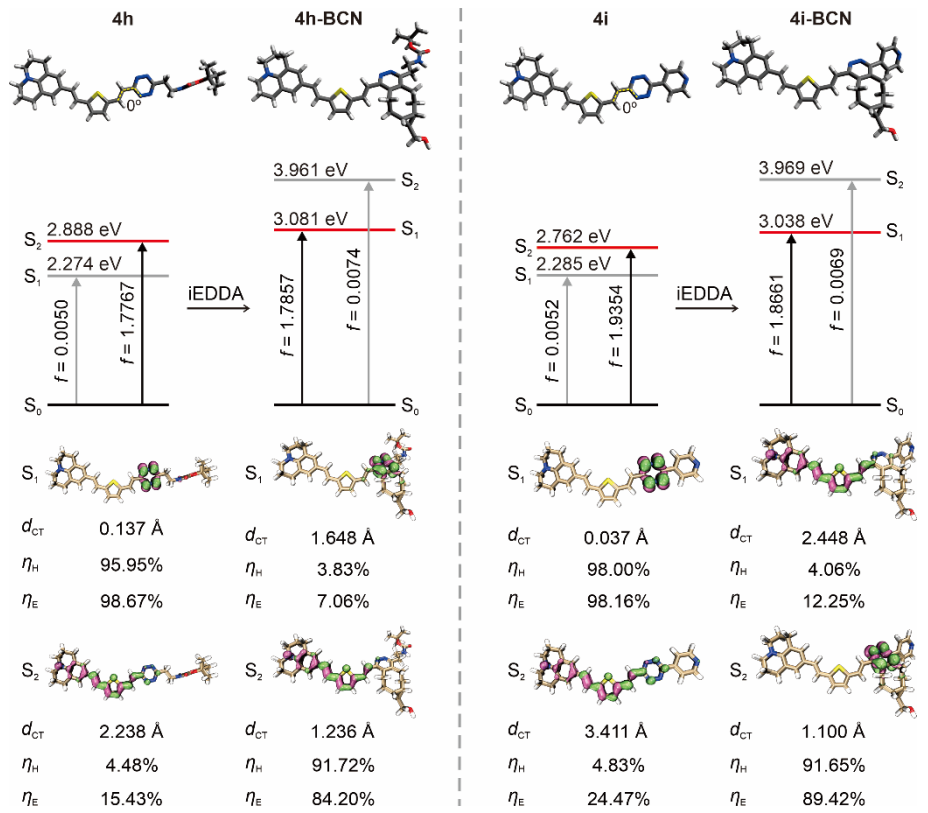

Fig. S13 Optimized geometries (top), energy levels of key states during the vertical excitation processes (middle), and corresponding hole-electron distributions (mauve: hole; green: electron) with d_{CT}, η_H, and η_E (bottom) of **4h**/**4h-BCN** (left) and **4i**/**4i-BCN** (right).

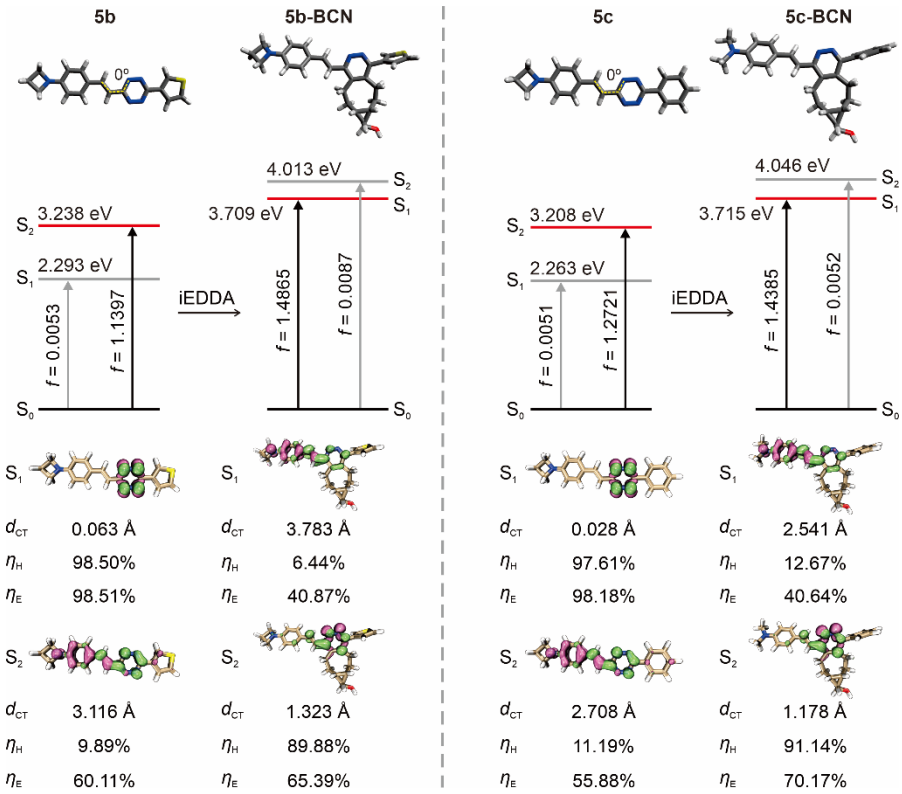

Fig. S14 Optimized geometries (top), energy levels of key states during the vertical excitation processes (middle), and corresponding hole-electron distributions (mauve: hole; green: electron) with d_{CT}, η_H, and η_E (bottom) of **5b**/**5b-BCN** (left) and **5c**/**5c-BCN** (right).

Comparison with the Energy Transfer to a Dark State (ETDS) Model

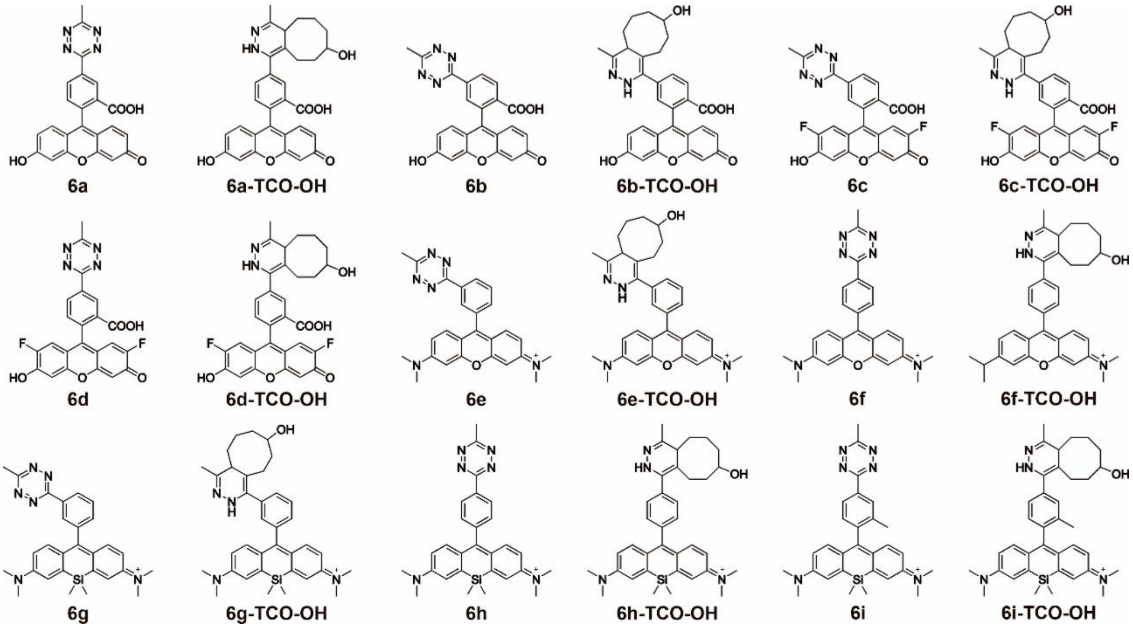

Fig. S15 Molecular structures of different tetrazine-derived probes reported by Wombacher *et al*. before and after reacting with *trans*-cyclooctenol (**TCO-OH**).[18]

Table S2. Properties of Labels **6a-i** and their products (after iEDDA reactions with **TCO-OH**).

Before the iEDDA reactions		After the iEDDA reactions			
Molecule	ΔE (eV)[19]	Molecule	Peak λ_{em} (nm)[18]	FE ratio[18]	Quantum yield (QY)[18]
6a	0.9875	**6a-TCO-OH**	521	72-fold	0.266
6b	0.9854	**6b-TCO-OH**	517	109-fold	0.360
6c	0.9881	**6c-TCO-OH**	522	103-fold	0.422
6d	0.9901	**6d-TCO-OH**	524	60-fold	0.288
6e	0.5870	**6e-TCO-OH**	577	12-fold	0.372
6f	0.5620	**6f-TCO-OH**	580	22-fold	0.814
6g	0.1661	**6g-TCO-OH**	664	3.7-fold	0.063
6h	0.1675	**6h-TCO-OH**	665	1.8-fold	0.036
6i	0.1607	**6i-TCO-OH**	666	2-fold	0.052

Table S3. Properties of probes **4a-i** and their products (after iEDDA reactions with **BCN**).

Before the iEDDA reactions		After the iEDDA reactions			
Molecule	ΔE (eV)	Molecule	Peak λ_{em} (nm)[3]	FE ratio[3]	QY[3]
4a	0.983	**4a-BCN**	556	186-fold	0.14
4b	0.912	**4b-BCN**	587	265-fold	0.29
4c	0.700	**4c-BCN**	622	277-fold	0.18
4d	0.670	**4d-BCN**	642	961-fold	0.30
4e	0.597	**4e-BCN**	652	304-fold	0.14
4f	0.636	**4f-BCN**	650	692-fold	0.17
4g	0.542	**4g-BCN**	685	910-fold	0.18
4h	0.614	**4h-BCN**	688	666-fold	0.14
4i	0.477	**4i-BCN**	728	400-fold	0.07

Design Strategies for ICDS-Based Fluorogenic Labels

Table S4. Calculated energies of the dark states in different ICDS labels.

Molecule	The vertical excitation energy of the dark state (eV)	Average (eV)
2a'	2.269	2.279
2b'	2.268	
2c'	2.267	
2d'	2.264	
3a	2.274	
3b	2.275	
3c	2.277	
3d	2.274	
3e	2.275	
4a	2.279	
4b	2.279	
4c	2.279	
4d	2.280	
4e	2.316	
4f	2.275	
4g	2.286	
4h	2.274	
4i	2.285	
5a	2.293	
5b	2.293	
5c	2.263	
5d	2.282	

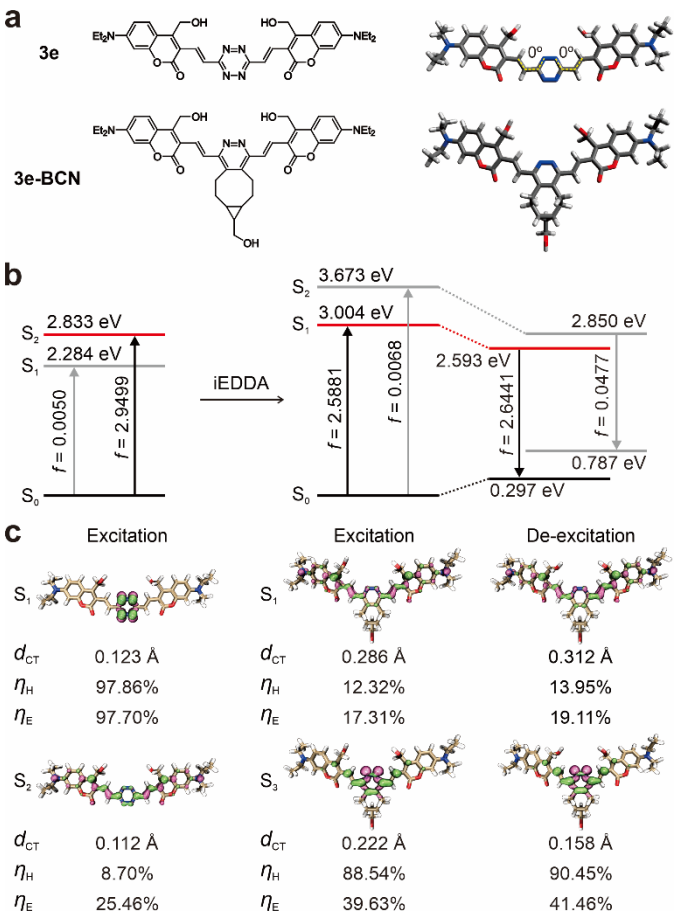

Fig. S16 (a) Molecular structures, optimized geometries, (b) energy levels of key states during the excitation and de-excitation processes, and (c) corresponding hole-electron distributions (mauve: hole; green: electron) with d_{CT}, η_H, and η_E of **3e** and **3e-BCN**.

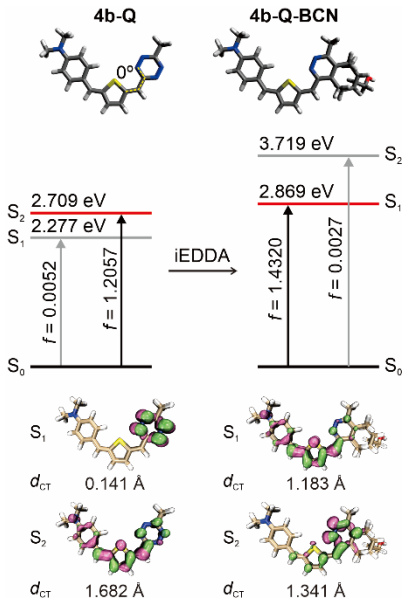

Fig. S17 Optimized geometries (top), energy levels of key states during the vertical excitation processes (middle), and corresponding hole-electron distributions (mauve: hole; green: electron) with d_{CT} (bottom) of **4b-Q**/**4b-Q-BCN**.

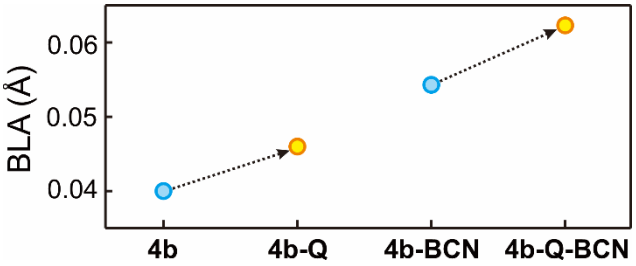

Fig. S18 Bond-length alternation values for **4b**, **4b-BCN**, **4b-Q**, and **4b-Q-BCN** (calculated along the highlighted paths in the π-conjugation bridges in Fig. 8a) at the ground state.

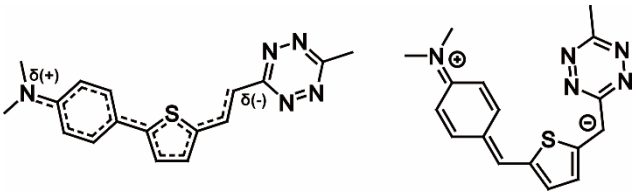

Fig. S19 Representative resonance structures of **4b** and **4b-Q**.

We calculated the bond-length alternation (BLA) values based on the ground state geometries for these four molecules along the highlighted paths in the *π*-conjugation bridges (Fig. 7a). The BLA values of **4b-Q** and **4b-Q-BCN** are larger than those of **4b** and **4b-BCN** (Fig. S18), indicating that the products after swapping the thiophene and methine units have stronger quinoidal characteristics. The resonance structure of **4b** can be illustrated by a delocalized structure with a partially spread charge distribution, whereas **4b-Q** can be described by a polarized structure with large charge separation (Fig. S19). Hence, **4b-Q** is more polarized in comparison to **4b** at S_0.

We next constructed the electrostatic potential (ESP) surfaces of **4b** and **4b-Q** with a focus on the partial charge separations on the diethylamino group (donor; Q_D) and the tetrazine unit (acceptor; Q_A; Fig. S20). In good agreement with the BLA analysis, more positive charges are distributed on the donor of **4b-Q** (Q_D = 0.131 e) than that on **4b** (Q_D = 0.113 e). Moreover, **4b** has less substantial negative potential on the tetrazine group (Q_A = -0.431 e) than **4b-Q** does (Q_A = -0.452 e). Owing to the stronger electron-donating/withdrawing strength, **4b-BCN** demonstrates a stabilized S_2 during the vertical excitation (Fig. S17).

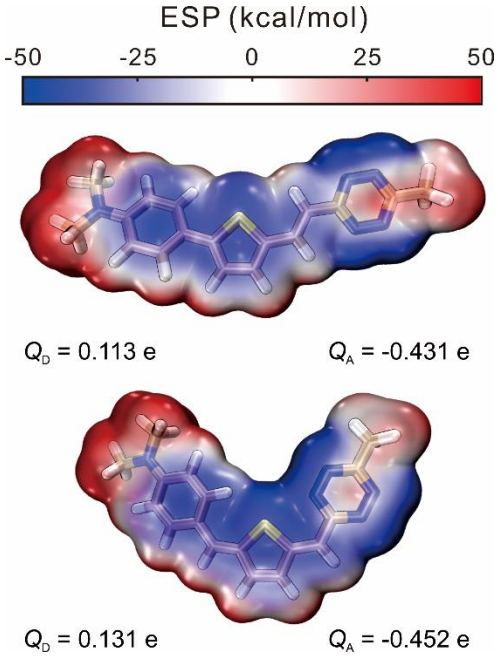

Fig. S20 Electrostatic potential surfaces of **4b** (top) and **4b-Q** (bottom) with partial charge value at donor and acceptor.

We also compared the d_{CT} of **4b** and **4b-BCN** in the Frank-Condon states (Fig. S21). Due to the enhanced charge separation of **4b-BCN** at S_0, this molecule shows a weaker d_{CT} = 1.682 Å during the photoexcitation from S_0 to S_2 compared to **4b** (d_{CT} = 2.148 Å). Therefore, our results show that exchanging the connection orders in the π-conjugation bridges can give the molecule strong quinoidal characteristics for strengthening the charge separation at S_0. This method thus effectively induces the spectral redshift in the resulting dyes.

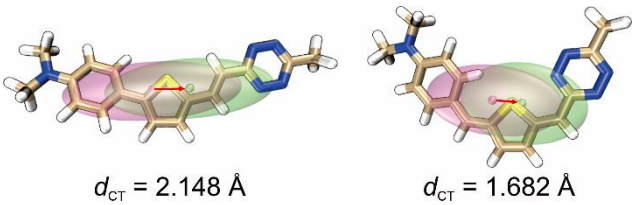

Fig. S21 Centroid hole-electron distributions with charge transfer directions and distances of **4b** (left) and **4b-Q** (right; mauve: hole; green: electron).

Limitation of the ICDS Mechanism

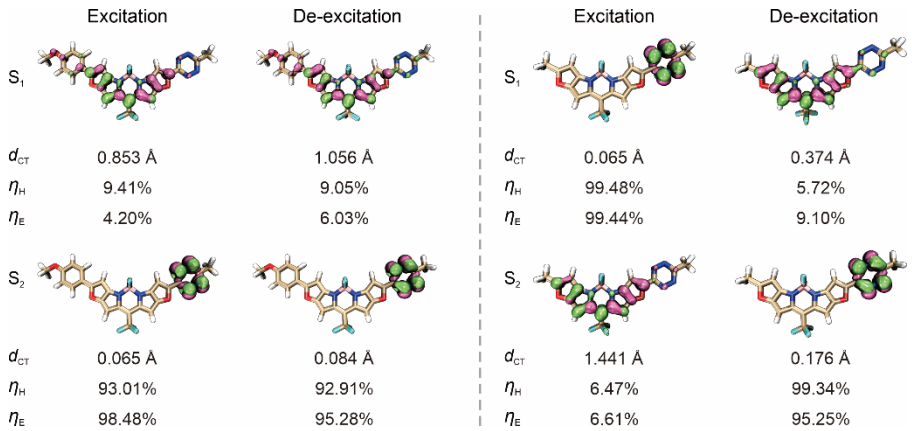

Fig. S22 Hole-electron distributions (mauve: hole; green: electron) with d_{CT}, η_H, and η_E of **7a** (left) and **7b** (right).

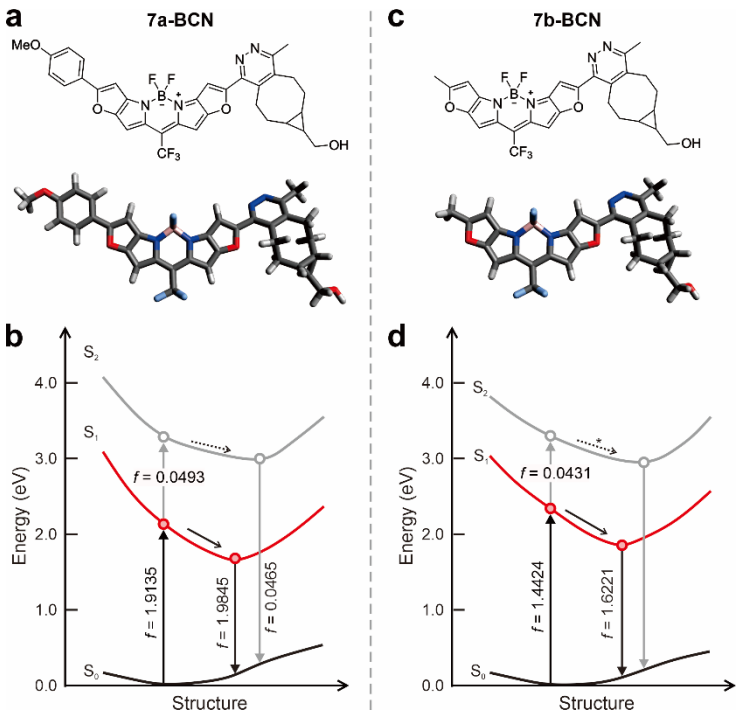

Fig. S23 Molecular structures, optimized geometries (a and c), energy levels of key states during the excitation and de-excitation processes (b and d) of **7a-BCN** (left) and **7b-BCN** (right; * means that the geometric relaxation process was not optimized).

References

1 Y. Lee, W. Cho, J. Sung, E. Kim and S. B. Park, Monochromophoric Design Strategy for Tetrazine-Based Colorful Bioorthogonal Probes with a Single Fluorescent Core Skeleton, *J. Am. Chem. Soc.*, 2018, **140**, 974-983.

2 M. Bojtar, K. Nemeth, F. Domahidy, G. Knorr, A. Verkman, M. Kallay and P. Kele, Conditionally Activatable Visible-Light Photocages, *J. Am. Chem. Soc.*, 2020, **142**, 15164-15171.

3 W. Mao, J. Tang, L. Dai, X. He, J. Li, L. Cai, P. Liao, R. Jiang, J. Zhou and H. Wu, A General Strategy to Design Highly Fluorogenic Far-Red and Near-Infrared Tetrazine Bioorthogonal Probes, *Angew. Chem., Int. Ed.*, 2021, **60**, 2393-2397.

4 S. J. Siegl, J. Galeta, R. Dzijak, M. Dracinsky and M. Vrabel, Bioorthogonal Fluorescence Turn-On Labeling Based on Bicyclononyne-Tetrazine Cycloaddition Reactions that Form Pyridazine Products, *ChemPlusChem*, 2019, **84**, 493-497.

5 A. D. Becke, Density-Functional Thermochemistry. III. The Role of Exact Exchange, *J. Chem. Phys.*, 1993, **98**, 5648-5652.

6 G. Scalmani, M. J. Frisch, B. Mennucci, J. Tomasi, R. Cammi and V. Barone, Geometries and Properties of Excited States in the Gas Phase and in Solution: Theory and Application of a Time-Dependent Density Functional Theory Polarizable Continuum Model. *J. Chem. Phys.*, 2006, **124**, 94107.

7 M. J. Frisch, G. W. Trucks, H. B. Schlegel, G. E. Scuseria, M. A. Robb, J. R. Cheeseman, G. Scalmani, V. Barone, G. A. Petersson, H. Nakatsuji, X. Li, M. Caricato, A. V. Marenich, J. Bloino, B. G. Janesko, R. Gomperts, B. Mennucci, H. P. Hratchian, J. V. Ortiz, A. F. Izmaylov, J. L. Sonnenberg, D. Williams-Young, F. Ding, F. Lipparini, F. Egidi, J. Goings, B. Peng, A. Petrone, T. Henderson, D. Ranasinghe, V. G. Zakrzewski, J. Gao, N. Rega, G. Zheng, W. Liang, M. Hada, M. Ehara, K. Toyota, R. Fukuda, J. Hasegawa, M. Ishida, T. Nakajima, Y. Honda, O. Kitao, H. Nakai, T. Vreven, K. Throssell, J. A. Montgomery, Jr., J. E. Peralta, F. Ogliaro, M. J. Bearpark, J. J. Heyd, E. N. Brothers, K. N. Kudin, V. N. Staroverov, T. A. Keith, R. Kobayashi, J. Normand, K. Raghavachari, A. P. Rendell, J. C. Burant, S. S. Iyengar, J. Tomasi, M. Cossi, J. M. Millam, M. Klene, C. Adamo, R. Cammi, J. W. Ochterski, R. L. Martin, K. Morokuma, O. Farkas, J. B. Foresman, and D. J. Fox, Gaussian 16, Gaussian, *Inc., Wallingford CT*, 2016.

8 J. D. Chai and M. Head-Gordon, Long-Range Corrected Hybrid Density Functionals with Damped Atom-Atom Dispersion Corrections, *Phys. Chem. Chem. Phys.*, 2008, **10**, 6615-6620.

9 F. Weigend and R. Ahlrichs, Balanced Basis Sets of Split Valence, Triple Zeta Valence and Quadruple Zeta Valence Quality for H to Rn: Design and Assessment of Accuracy, *Phys. Chem. Chem. Phys.*, 2005, **7**, 3297-3305.

10 A. V. Marenich, C. J. Cramer and D. G. Truhlar, Universal Solvation Model Based on Solute Electron Density and on a Continuum Model of the Solvent Defined by the Bulk Dielectric Constant and Atomic Surface Tensions, *J. Phys. Chem. B*, 2009, **113**, 6378-6396.

11 K. V. Mikkelsen, P. Jo/rgensen and H. J. r. A. Jensen, A Multiconfiguration Self-Consistent Reaction Field Response Method, *J. Chem. Phys.*, 1994, **100**, 6597-6607.

12 M. Caricato, B. Mennucci, J. Tomasi, F. Ingrosso, R. Cammi, S. Corni and G. Scalmani, Formation and Relaxation of Excited States in Solution: A New Time Dependent Polarizable Continuum Model Based on Time Dependent Density Functional Theory, *J. Chem. Phys.*, 2006, **124**, 124520.

13 M. D. Hanwell, D. E. Curtis, D. C. Lonie, T. Vandermeersch, E. Zurek and G. R. Hutchison, Avogadro: An Advanced Semantic Chemical Editor, Visualization, and Analysis Platform, *J. Cheminform.*, 2012, **4**, 1-17.

14 T. Le Bahers, C. Adamo and I. Ciofini, A Qualitative Index of Spatial Extent in Charge-Transfer Excitations, *J. Chem. Theory Comput.*, 2011, **7**, 2498-2506.

15 Z. Liu and T. Lu, Optical Properties of Novel Conjugated Nanohoops: Revealing the Effects of Topology and Size, *J. Phys. Chem. C*, 2020, **124**, 7353-7360.

16 T. Lu and F. Chen, Multiwfn: A Multifunctional Wavefunction Analyzer., *J. Comput. Chem.*, 2012, **33**, 580-592.

17 W. Humphrey, A. Dalke and K. Schulten, VMD: Visual Molecular Dynamics, *J. Mol. Graph.*, 1996, **14**, 33-38.

18 A. Wieczorek, P. Werther, J. Euchner and R. Wombacher, Green- to Far-Red-Emitting Fluorogenic Tetrazine Probes - Synthetic Access and No-Wash Protein Imaging inside Living Cells, *Chem. Sci.*, 2017, **8**, 1506-1510.

19 W. Chi, L. Huang, C. Wang, D. Tan, Z. Xu and X. Liu, A Unified Fluorescence Quenching Mechanism of Tetrazine-Based Fluorogenic Dyes: Energy Transfer to a Dark State, *Mater. Chem. Front.*, 2021, **5**, 7012-7021.